

# AN ELECTROSTATICALLY-ACTUATED ROTATIONAL MICROMIRROR

M. J. Jaasma and R. E. Sanchez

Department of Mechanical Engineering, University of California, Berkeley, CA.

**Abstract** An in-plane optical switch was designed by incorporating a micromirror with a rotational comb drive. The comb drive is capable of both actuation and angular position sensing. The optical switch measures 2.0 mm in diameter and can perform in-plane reflection of up to 90° at 30 V. The system is mechanically overdamped, having a rise time for scanning of 7.0 ms and a natural frequency of 88 Hz. Given the high scanning range at low voltage, if rotational scanning at low frequency is desired (<45 Hz), the rotational comb drive is an excellent candidate for combined actuation and sensing.

## 1. Introduction

MEMS microactuators have potential in applications that involve transmitting electromagnetic, acoustic, and light energy [1]. An optical switch device can be created by incorporating a micromirror with a microactuator. Out-of-plane reflection can be obtained via torsional rotation of a horizontal mirror [1, 2]. One limitation to this design is the limited range of motion, which is typically less than 20°. In-plane reflection can be obtained by angular rotation of a vertical mirror. Several DRIE-fabricated devices have been successfully developed for such in-plane scanning via electrostatic actuation [3-5].

The rotational comb drive was first introduced by Tang *et al.* [6], but to our knowledge this actuation method has not been used in an optical switch design. One key advantage of the rotational comb drive is the ability to both actuate and sense position in one device. This can be realized for a large range of angular displacements. Fine position control can be accomplished with well-established control theory.

The overall goal of this study was to design an electrostatically-actuated rotational micromirror capable of in-plane reflection of a laser beam up to 90° from its original direction (45° mirror rotation). Specific design goals included minimization of device size, required voltage, and scanning time.

The rotational micromirror device will be fabricated using the Sandia Ultra-planar, Multi-level MEMS Technology (SUMMiT V) fabrication process at Sandia National Laboratories. The SUMMiT V process is a five-level polycrystalline silicon surface micromachining process. The five polysilicon layers are low-stress, vary in thickness (0.3, 1.0, 1.5, 2.25, and 2.25 μm), and are separated by sacrificial layers of silicon dioxide. The oxide layers separating the top three polysilicon layers are planarized via Chemical-Mechanical Polishing (CMP). The top polysilicon layer is also coated with a 0.7 μm film of Al/Cu.

## 2. Design

### 2.1 Comb drive actuation

The rotational comb drive consists of eight sets of overlapping comb fingers (see Fig. 1) that form four capacitors. In each capacitor, one set of fingers is anchored to the substrate, while the other is free to rotate through the overlapping region. The two outer comb drives (outer half of fingers) are used for actuation. Imposing a voltage,  $V$ , on one anchored set causes a tangential force to act on the adjacent free set. The total moment acting on the free set is:

$$M_{total} = \epsilon_0 V^2 \frac{t}{g} \alpha \sum_{i=1}^n r_i \quad \text{Eq (1)}$$

where  $t$  is the film thickness,  $g$  is the gap thickness,  $\alpha$  is the fringe factor,  $n$  is the total number of fingers, and  $r$  is the finger radius. The device was designed to have a maximum applied voltage of 30 V, which corresponds to the maximum angular displacement of 45°. Given a  $t/g$  ratio of 0.56, the fringe factor was assumed to be 1.75.

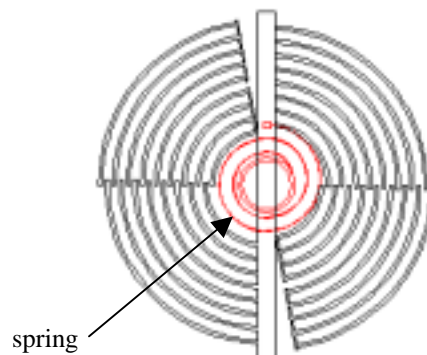


**Fig. 1.** Top view of the device showing the comb drives, spring, and mirror supporting plate (mirror not pictured). Total diameter is 2.0 mm. For illustrative purposes, all fingers are not shown.

### 2.2 Capacitive sensing

In addition to the actuation comb drives, the inner two comb drives (inner half of fingers) are used to sense angular displacement (see Fig. 1). Capacitance is measured using a one-active Wheatstone bridge with a 1.0 V excitation. Non-

variable capacitors are 500 fF. Capacitance,  $C$ , is related to angular displacement:

$$C = \frac{2\epsilon_0 t}{g} (\theta + \beta) \sum_{i=1}^n r_i \quad \text{Eq (2)}$$

where  $\beta$  is the angular overlap at  $\theta=0$ .

### 2.3 Motion

The angular motion of the mirror/comb drive system is governed by the second order mechanical system equation of motion [7]:

$$J\ddot{\theta} + b\dot{\theta} + k_\theta\theta = M \quad \text{or} \quad \ddot{\theta} + 2\zeta\omega_n\dot{\theta} + \omega_n^2\theta = \frac{M}{J} \quad \text{Eq (3)}$$

where  $J$  is the mass moment of inertia,  $b$  is the damping coefficient,  $k_\theta$  is the torsional spring constant,  $M$  is the applied moment,  $\zeta$  is the damping factor, and  $\omega_n$  is the torsional natural frequency.

In this device, the damping coefficient,  $b$ , is mainly a measure of the air resistance to motion. Air resistance on the comb drive fingers was estimated by assuming Couette flow between the fingers and substrate. Since the finger velocity depends on radial position,  $b$  is estimated from the air viscosity,  $\mu$ , and thickness,  $h$ :

$$b\dot{\theta} = \int \tau r dA = \int_{r_{\min}}^{r_{\max}} \frac{\pi\mu\dot{\theta}r^3}{h} dr \quad \text{Eq (4)}$$

The drag force acting on the mirror alone was found to be two orders of magnitude smaller than that due to Couette damping and was neglected.

The mirror is supported rotationally by an Archimedean spring, which has a spring constant of:

$$k_\theta = \frac{Etw^3}{12L} \quad \text{Eq (5)}$$

where  $E$  is Young's modulus,  $w$  is the width of the spring, and  $L$  is the total spring length [8].

The total moment acting on the rotating mirror structure is the actuation moment minus the frictional moment (dynamic) due to the plate surface rotating on the underlying polysilicon support. This frictional moment was estimated based on the dynamic coefficient of friction and the weight of the suspended components. The dynamic coefficient of friction was assumed to be 0.7 [9]. This frictional moment was also used as a low estimate of the static friction moment acting on the resting structure.

### 2.3 Fabrication

The proposed structure is fabricated using the SUMMiT V process. Of the five polysilicon layers, the first is an electric interconnect layer while the other four are mechanical layers. This process is the only one that offers CMP to eliminate inter-level interference. This is the main reason that the SUMMiT V process was chosen since the proposed design produces interferences when one of the sacrificial layers cannot be planarized. Note that the

proposed design is process oriented. Once the SUMMiT V process was chosen, the initial design was modified to match this process. Our design can also be fabricated with a custom process that includes three layers of polysilicon with interlaying planarized sacrificial layers.

After initial layers of silicon dioxide, silicon nitride, polysilicon (MMPoly0) (Fig. 2a), and TEOS (SacOx1) are deposited, polysilicon (MMPoly1) is deposited over the SacOx1 layer (Fig. 2b). This layer will connect to MMPoly0, establishing the electrical connections. This layer is then patterned and etched (with RIE). SacOx1 is then partially etched (using HF). This etches under the MMPoly1 and creates flanged geometry in the pin-joint and around the hub when subsequent layers of oxide and polysilicon are added (Fig. 2). A 0.5  $\mu\text{m}$  layer of SacOx2 is added following the MMPoly1. This SacOx2 layer provides a conformal coating both on the top of MMPoly1 and around the inside of the hub. Since this layer is only 0.5  $\mu\text{m}$  thick, it does not completely fill the undercut regions, leaving space for the next layer of poly that forms a flange (Fig. 2c). Following the cut of the SacOx1, a 1  $\mu\text{m}$  thick layer of MMPoly2 is deposited (Fig. 2d). This layer of MMPoly2 fills the undercut regions below MMPoly1 to form the flanges for the pin-joint. After the deposition of MMPoly2 the composite layer of MMPoly1 and MMPoly2 are etched. The torsional spring is also formed in this step. A layer of SacOx3 is then deposited, planarized, patterned, and etched. The etching provides the connection to the spring and to the shaft. A 2  $\mu\text{m}$  layer of MMPoly3 is then deposited, patterned, and etched (Fig. 2e). Figure 1 shows the top view after this step is performed.

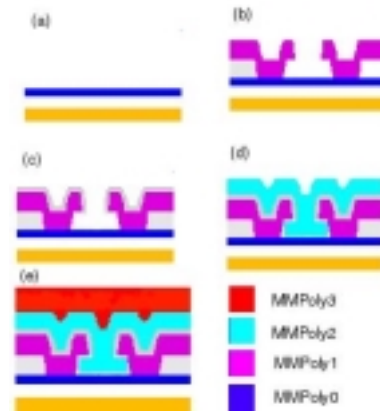


**Fig. 2.** Device cross-sections showing fabrication steps of the pin-joint and hub. The rotating structure is composed of MMPoly2 and MMPoly3.

The micromirror is fabricated separately. This can also be done using the SUMMIT V process among other simpler processes. Here, the fifth polysilicon layer is the mirror structural layer. It is coated with 0.7  $\mu\text{m}$  Al/Cu to improve reflectivity. The mirror measures 200 X 200 X 2.95  $\mu\text{m}$  with two posts protruding from the bottom. These posts are coated with glue, and using a micromanipulator, the mirror is attached to the device by placing the posts in the appropriate etch holes (see Fig. 1).

#### 2.4 Radial beam deflection

If the actuation comb drive is slightly misaligned radially, a force will result perpendicular to each finger. In turn, if the finger's flexural stiffness is not sufficiently high, two adjacent fingers in the comb drive will bend and make contact. This will cause the structure fail because the rotating structure will obtain the applied voltage.

The pin of the rotating table is designed to have a clearance of approximately 0.5 $\mu\text{m}$  with respect to the substrate posts that constrain it. Thus, the beam can be located  $\pm 0.5\mu\text{m}$  from the center distance of the two plates. For one finger, the electrostatic force in the radial direction due to the misalignment of the plate is:

$$F = \left[ \left( -\frac{1}{2} \epsilon_0 V^2 \frac{t \cdot R \theta}{(z_1)^2} \right) - \left( -\frac{1}{2} \epsilon_0 V^2 \frac{t \cdot R \theta}{(z_2)^2} \right) \right] \quad \text{eq(6)}$$

The maximum force will be obtained when the angle is at its maximum, 45°.

The deflection of the curved beam is obtained using energy principals. Assuming that the deflection of the beam is due only to normal stresses, and not to shearing stresses:

$$U = 6 \int_0^\theta \frac{M^2 R}{I \cdot E} d\theta \quad \text{Eq (7)}$$

Once the strain energy has been obtained, the deflection of the beam can be obtained by Castigliano's theorem [10]:

$$y = \frac{\partial U}{\partial P} = 6 \int_0^\theta \frac{w R^4 \theta^3}{EI} d\theta = \frac{3}{2} \left( \frac{R^4}{EI} w \theta^4 \right) \quad \text{Eq (8)}$$

where w is the force over the angle.

### 3. Test Structures

Several tests will need to be conducted to determine frictional factors as well as to validate our theoretical calculations.

#### 3.1 Static friction moment

To position the micromirror from the initial resting position, the moment due to static friction between the plate and the underlying hub will need

to be overcome. To determine this frictional moment, we will slowly ramp up the voltage applied to the actuating fingers until the rotor breaks free. Based on the derived moment/voltage relationship (Fig. 3), the static friction moment can be calculated.

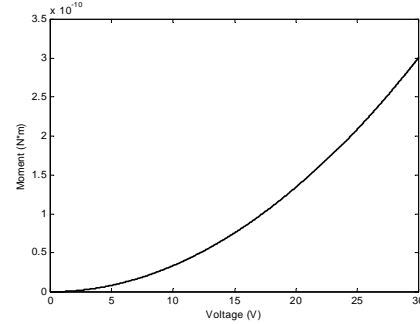


**Fig. 3.** Applied moment vs. applied voltage. This relationship will be used to determine the static friction moment.

#### 3.2 Natural frequency calculations

First, the natural frequency will be experimentally obtained by driving the system with a nominal voltage at varying frequency. Once the time data of the reference voltage and output displacement are collected, the frequency content of these data can be obtained by performing a Fast Fourier Transform (FFT). Second, mass moment of inertia and natural frequency calculations will be validated by analyzing the change in natural frequency with varying comb finger width (Fig. 4a). This analysis was simplified by setting the gap thickness equal to the finger width.

#### 3.3 Radial comb finger deflection

Radial comb finger deflection will be experimentally analyzed for varying finger widths. This will be compared against theoretical calculations (Fig. 4b). Finger deflection will be measured with an optical microscope.

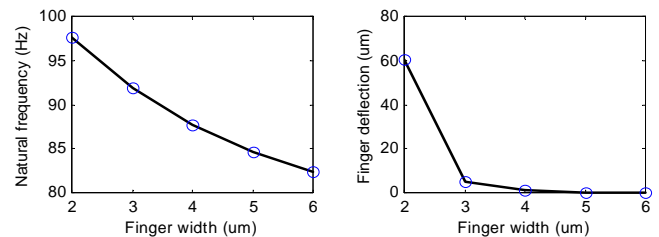


**Fig. 4.** (a) Change in natural frequency due to change in comb finger width. (b) Radial finger deflection vs. finger thickness at an applied voltage of 30 V.

### 3.4 Minimum comb finger overlap

Test structures will be fabricated with varying comb finger overlap to determine the minimum overlap length needed for actuation.

### 3.5 Damping factor

The vibration damping factor,  $\zeta$ , will need to be experimentally determined in order to know the time necessary to scan from one position to another. The measured damping coefficient, which encompasses all dynamic friction due to air and surface roughness effects, can also be compared against the theoretically derived coefficient to evaluate the accuracy of our models. We will measure the damping coefficient by comparing the actual and theoretical angular displacement vs. time when 30 V is applied to the actuator.

## 4. Expected Results

The calculated mass moment of inertia and natural frequency were  $1.26e-15 \text{ kg}\cdot\text{m}^2$  and 88 Hz, respectively. Our calculations indicated that the system is mechanically overdamped, having a damping coefficient of 1.94. Thus, the system will not oscillate while attaining its final angular displacement (Fig. 5a). The rise time is 7.0 ms. A nonlinear relationship was found between actuator voltage and final angular displacement (Fig. 5b). A linear relationship was found between sensor capacitance and displacement (Fig. 5c).

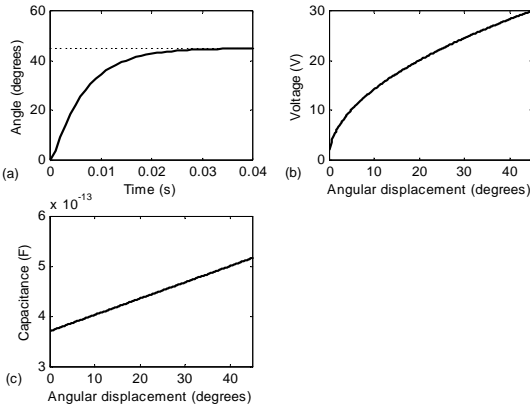


**Fig. 5.** (a) Angular displacement vs. time for actuation to a final displacement of  $45^\circ$ ; (b) Applied actuator voltage vs. desired angular displacement. (c) Capacitance vs. angular displacement for capacitive sensing.

## 5. Conclusions

We have design a rotational optical switch that is capable of in-plane beam reflection of up to  $90^\circ$

while only requiring an input voltage of 30 V. The large scanning range at such a low voltage is a major strength of this design. The high reflectivity of the Al/Cu coating on the micromirror should minimize signal loss. Based on our calculations, we believe that the device will operate effectively without use of the sensing comb drive. However, incorporation of real-time control measures with the angular displacement sensing should increase the efficiency and accuracy of the device. In addition, the capacitance of the sensing comb drive should be high enough to achieve precise sensing capabilities.

Our design has several limitations. One limitation is the theoretically low natural frequency. To avoid resonance problems, the device should be operated no higher than 45 Hz. Many optical switch applications require high scanning speed, which would limit the usefulness of our device. However, if we operate the device at higher voltage, a higher torsional spring constant can be used, which can increase the natural frequency substantially. A second limitation is the theoretically high friction on the device during scanning. Our calculations indicate that the system is overdamped, which reduces the scanning speed, but is also advantageous for oscillation-free motion. These calculations will need to be verified experimentally before final conclusions can be drawn.

The strengths of this optical switch design are largely due to the advantages of the rotational comb drive in actuation and sensing. This makes the rotational comb drive a candidate for many other applications, which include a disk drive read/write head and an angular transducer.

## 6. References

- [1] Jerwei H, Weileun F, 2000. Sensors and Actuators A 79:64-70.
- [2] Camon H, Larnaudie F, 2000. IEEE Conference Proceedings, p. 645-50.
- [3] Marxer C, Thio C, Gretillat MA, de Rooij NF, Baettig R, Anthamatten O, Valk V, Vogel P, 1997. Journal of Microelectromechanical Systems 6:277-285.
- [4] Yasseen AA, Mitchell JN, Klemic JF, Smith DA, Mehregany M, 1999. IEEE Journal of Selected Topics in Quantum Electronics 5:26-32.
- [5] Yasseen AA, Mitchell JN, Smith DA, Mehregany M, 1999. Sensors and Actuators 77:73-79.
- [6] Tang WC, Nguyen TH, Howe RT, 1989. Sensors and Actuators 20:25-32.
- [7] Meriam JL, Kraige LG, 1997. Dynamics, 4 ed., Wiley, New York.
- [8] Wahl AM, 1945. Mechanical springs, 1 ed. Penton, Cleveland.
- [9] Smith BK, Sniegowski JJ, LaVigne G, Brown C, 1998. Sensors and Actuators A 70:159-163.
- [10] Beer FP, Johnston ER, 1981. Mechanics of Materials, 1 ed. McGraw-Hill, New York.